

Hydrophilic poly-ether side-chained benzodithiophene-based homopolymer for solar cells and field-effect transistors

Qian Liu · Xichang Bao · Yan Yan ·
Zhengkun Du · V. A. L. Roy · Dangqiang Zhu ·
Mingliang Sun · Chun Sing Lee · Renqiang Yang

Received: 27 October 2014 / Accepted: 12 December 2014 / Published online: 24 December 2014
© Springer Science+Business Media New York 2014

Abstract Two benzodithiophene (BDT)-based homopolymers which have different mole ratios of poly-ether side chain substitute were synthesized by Stille coupling reaction. The polymers show decomposition temperature (T_d) around 317 °C and optical band gap around 2.2 eV. Solar cell devices with bulk heterojunction structure and field-effect transistors devices were fabricated to evaluate the photovoltaic properties of resultant polymers. Solar cell devices based on the polymer with 100 % poly-ether side chain (P1) show low power conversion efficiencies (PCEs) of 0.71 % resulting from the poor morphology of active layer which has rough surface and fairly large domain size due to the high aggregation tendency of P1:PCBM ([6,6]-phenyl-C61-butyric acid methyl ester) blend thin film as active layer in the structure of devices. Polymer with alternating poly-ether and alkoxy chained BDT (P2) and PCBM blend film shows smooth surface and appropriate domain size, which help to enhance the hole transportation and photovoltaic performances. The PCEs of the devices

based on P2 reached 2.00 % which is a decent result for BDT-based homopolymer donor with relatively large band gap (ca. 2.2 eV). These two polymers exhibited mobilities of 3.95×10^{-4} and 6.18×10^{-4} cm²/Vs in field-effect transistors, respectively.

Introduction

Bulk heterojunction (BHJ) polymer solar cells (PSCs) based on π -conjugated (semiconducting) polymers and fullerene derivatives have attracted much attention as a promising candidate for clean and renewable solar energy conversion technologies because of their advantages, such as low cost, flexibility, and solution processing [1–6]. During the past decades, tremendous efforts have been devoted to develop novel conjugated polymers with different alternating units along the polymer backbone, and the power conversion efficiencies (PCEs) of PSCs based on these polymers have been improved from about 1 % to more than 9 % [7–12]. For example, donor–acceptor conjugated polymers with alternating electron-rich (donor) and electron-deficient (acceptor) units can achieve appropriate band gap and energy level by controlling the intramolecular charge transfer (ICT) from donor to acceptor moieties. This kind of polymers can achieve relatively high photovoltaic performance [8]. However, some recent studies have begun to focus on the effect of different side chains on conjugated polymers with the same backbone sequence. Although the side chains have minimal impact on the observed band gap and energy levels of the polymer, appropriate side chains can improve the polymer solubility, molecular weight, mobility, π – π stacking, and the morphology of phase-separated blends which definitely will affect the device efficiencies [13–16].

Q. Liu · X. Bao · Z. Du · D. Zhu · R. Yang (✉)
CAS Key Laboratory of Bio-based Materials, Qingdao Institute
of Bioenergy and Bioprocess Technology, Chinese Academy of
Sciences, Qingdao 266101, Shandong, China
e-mail: yangrq@qibebt.ac.cn

Q. Liu · M. Sun (✉)
Institute of Materials Science and Engineering, Ocean University
of China, Qingdao 266100, Shandong, China
e-mail: mlsun@ouc.edu.cn

Y. Yan · V. A. L. Roy · M. Sun · C. S. Lee
Center of Super-Diamond and Advanced Films (COSDAF), City
University of Hong Kong, Kowloon Tong, Hong Kong

M. Sun
Shenzhen Research Institute, City University of Hong Kong,
High-Tech Zone, Nanshan District, Shenzhen, China

Andersson and Hou reported fluorene and dithien-2-yl-2,1,3-benzothiadiazole (DTBT)-based polymers (PF-DTBT) which have identical polymer backbone but different alkyl side chains. The relationship between side chain bulkiness and the measured PCEs was exposed. PF-DTBT with ethylhexyl and hexyl substitutes on fluorene unit exhibited PCE of 2.2 %, while BisDMO-PF-DTBT with 3,7-dimethyl-octyl substitutes showed a higher PCE of 4.5 % [17, 18]. The effects of side chain have also been systematically explored on one of the best polymer photovoltaic materials to date, P3HT [19–22]. Gadisa and co-workers studied the charge transport and photovoltaic characteristics of regioregular poly(3-alkylthiophene) (P3AT), including P3BT, P3PT, and P3HT [20]. The authors proposed that the longer side chain facilitated the PCBM clusters formation by establishing efficient electron-percolation pathways. Essentially, balanced electron/hole mobilities were obtained with proper phase separation, leading to a high fill factor. In another study of functionalized side chains with different amounts in P3HT by Janssen et al. [9], the authors clearly demonstrated the possibility to tune the performances of (P3HT-based) conjugated polymer donor materials by introducing the functionalized side chains in moderate amounts, and they showed that functionalized P3AT copolymers, obtained via post-polymerization protocols from the presented ester-functionalized P3ATs (affording alcohol and cinnamoyl moieties in the side chains), provide a considerably more stable active layer blend morphology upon prolonged thermal annealing compared to regular P3HT. In 2008, Hou and Yang reported primarily the synthesis and electronic properties of benzodithiophene (BDT)-based copolymers [23]. Since then, the BDT unit has become one of the most employed donor moieties for PSCs, and a variety of BDT-based copolymers with substantial PCEs of 5–8 % were designed and synthesized [24–35]. Despite these features, the research of side chains on BDT-based polymers is still in its infancy and most of the limited studies are focused on copolymers [13, 14, 16, 36]. Compared with copolymers, homopolymers have more simple structure and are more suitable for considering the effects of side chains. For example, Ferraris et al. explored the effect of the dialkoxy and dithioalkoxy side chains on BDT unit by comparing the computational calculations and experimental results of O-BDT homopolymer, S-BDT homopolymer, and S-BDT-alt-O-BDT copolymer. The replacement of the alkoxy groups with thioalkoxy groups lowered the HOMO energy of the homopolymer from -5.31 to -5.41 eV and consequently enhanced open circuit voltage (V_{oc}) and ultimately the PCEs were improved from 1.56 to 4.00 % which is comparable with PCBM and P3HT system (the best homopolymer solar cells donor) [37]. However, the dithioalkoxy side-chained BDT-based

homopolymer exhibited low FF value of 0.53 which can be enhanced by forming more reliable morphology of polymer:PCBM blend [20].

In this paper, two BDT-based homopolymers with different mole ratios of poly-ether side chain were synthesized by Stille coupling reaction. Polymer solar cell devices were fabricated with BHJ structure with the synthesized polymers as donor and PCBM as acceptor. Our preliminary results show that it is an effective way to modulate the morphology of donor and acceptor blend film by controlling the mole percentage of hydrophilic poly-ether side chain in BDT-based homopolymer donor.

Experimental section

Materials

Unless otherwise stated, all reagents and starting materials were used as commercially purchased without further purification. All air- and water-sensitive reactions were performed under argon atmosphere. Toluene and tetrahydrofuran (THF) were distilled from sodium with benzophenone as indicator, and *N,N*-dimethylformamide (DMF) was distilled from CaH_2 under argon atmosphere prior to use. Compounds 1 and 5 were synthesized according to the reported literature [23].

Characterization

^1H and ^{13}C NMR (Nuclear Magnetic Resonance) spectra were recorded on a Bruker Advance III600 (600 MHz) spectrometer. Thermogravimetric analysis (TGA) and differential scanning calorimetry (DSC) were conducted on TA-Q600 equipment. The Ultraviolet–Visible (UV–Vis) absorption spectra were recorded by Hitachi U-4100 spectrophotometer. Cyclic Voltammetry (CV) measurements were performed on a CHI660D electrochemical workstation. Atomic Force Microscope (AFM) images were acquired with Agilent-5400 scanning probe microscope with a Nanodrive controller in tapping mode with MikroMasch NSC-15 AFM tips with resonant frequencies ~ 300 MHz. X-ray diffraction (XRD) spectra were recorded on a Bruker D8 Advance.

Solar cell devices fabrication

Photovoltaic devices were fabricated on $15 \times 15 \text{ mm}^2$ indium-tin-oxide (ITO)-coated glass substrates with a layered structure of ITO/PEDOT:PSS/Polymer:PCBM/Ca/Al. The ITO-coated glass substrates were cleaned in an ultrasonic bath in ITO leaner, distilled water, acetone, distilled water, and isopropyl alcohol sequentially. The substrates

were then oxygen plasma treated for 20 min, spin coated with PEDOT:PSS at 4000 rpm, and dried under argon at 160 °C for 25 min. The polymer and PCBM were dissolved in deoxygenated anhydrous chloroform in the weight ratios from 2:1, 1:1, 1:2 respectively and stirred overnight in MBraun glovebox. An active layer consisting of the blend of polymer and PCBM was then spin coated on PEDOT:PSS at 3000 rpm. Typical concentration of the polymer:PCBM blending solution was 24 mg/mL in this work. Subsequently, Ca (10 nm) and Al (100 nm) were thermally evaporated at a vacuum of $\sim 2 \times 10^{-4}$ Pa on top of active layer as a cathode. Photovoltaic performance was characterized under illumination with an AM1.5 (100 mW/cm²) in a nitrogen atmosphere (<0.1 ppm H₂O and O₂), and current voltage curve was recorded by Keithley 2420.

Fabrication of field-effect transistors (FET) devices

Bottom-gate/top-contact transistors were fabricated on heavily *n*-doped silicon substrates (served as gate electrode) with 100 nm thermal oxide (SiO₂) layers. After standard cleaning (15 min ultrasonic process in acetone, isopropanol and DI-water, sequentially), 5 mg/mL polymer dissolved in chloroform were spin coated on SiO₂ substrates at a speed of 1200 rpm for 1 min. Then, substrates were annealed on a hot plate at 120 °C for 30 min. Afterward, a 100-nm-thick gold film was vacuum sublimed as source/drain electrodes on semiconductor surface through a shadow mask (channel length/width = 50/1000 μm) at a rate of 0.2 Å/s.

Synthesis of monomers and polymers

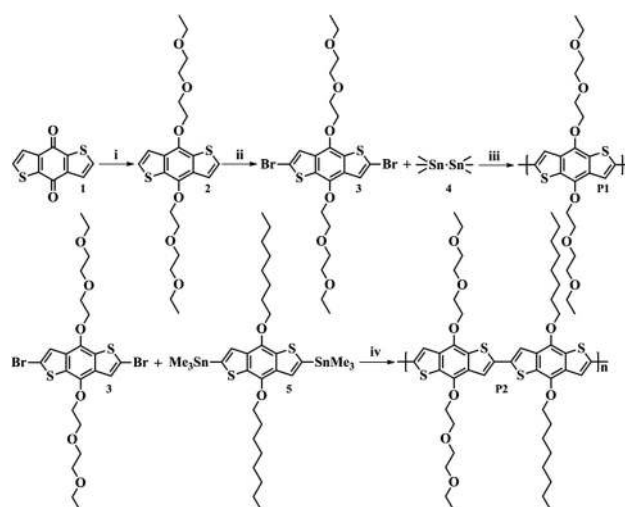
Synthesis of *E*-BDT (compound 2)

Under the protection of argon, benzo[1,2-*b*:4,5-*b'*]dithiophen-4,8-dione (compound 1, 1.1 g, 5 mmol), zinc powder (719 mg, 11 mmol), and 20 mL of distilled water were put into a 100 mL flask; then NaOH (3 g, 75 mmol) was added into the mixture. The mixture was stirred and heated to reflux for 1 h. During the reaction, the color of the mixture changed from yellow to red and then to origin. Subsequently, 1-(2-ethoxyethoxy)-2-bromoethane (2.96 g, 15 mmol) and a catalytic amount of tetrabutylammonium bromide (161 mg, 0.5 mmol) were added into the flask. After being refluxed for 6 h, the reactant was poured into cold water and extracted with diethyl ether. The ether layer was dried over by anhydrous MgSO₄. After removing the solvent, the crude product was purified by column chromatography using petroleum and acetic ether (2:1) as the eluent and then recrystallized from ethyl alcohol. *E*-BDT (compound 2) was obtained as a colorless crystal (1.89 g,

yield 83 %). ¹H NMR (CDCl₃, 600 MHz), δ (ppm): 7.58 (d, *J* = 5.4 Hz, 2H), 7.36 (d, *J* = 5.4 Hz, 2H), 4.44 (m, 4H), 3.88 (m, 4H), 3.75 (m, 4H), 3.65 (m, 4H), 3.56 (m, 4H), 1.23 (t, *J* = 6.6 Hz, *J* = 7.2 Hz, 6H).

Synthesis of *E*-BDT-Br (compound 3)

Under the protection of argon, compound 2 (1.82 g, 4 mmol) and 50 mL of THF were added into a 100 mL flask. The solution was cooled down to −78 °C and 5.5 mL of *n*-butyllithium (8.8 mmol, 1.6 M in *n*-hexane) was added dropwise. After being stirred at −78 °C for 2 h, a great deal of white solid precipitate appeared in the flask. Then, carbon tetrabromide (3.05 g, 9.2 mmol) was added in one portion and the reactant turned black but clear rapidly. Then the reactant was stirred at ambient temperature for another 2 h. Then, it was poured into 100 mL of cool water and extracted with diethyl ether. The organic layer was washed by water and dried by anhydrous MgSO₄. After removing the solvent under vacuum, the residue was purified by column chromatography using petroleum ether and acetic ether (2:1) as eluent and recrystallized from ethyl alcohol. 1.37 g of *E*-BDT-Br (compound 3) was obtained as a colorless needle crystal (2.24 mmol, yield 56 %). ¹H NMR (CDCl₃, 600 MHz) δ (ppm): 7.56 (s, 2H), 4.35 (m, 4H), 3.84 (m, 4H), 3.74 (m, 4H), 3.66 (m, 4H), 3.58 (m, 4H), 1.24 (t, *J* = 6.6 Hz, *J* = 7.2 Hz, 6H). ¹³C NMR (CDCl₃, 151 MHz), δ (ppm): 142.4, 131.4, 131.2, 123.4, 115.1, 73.1, 71.0, 70.3, 69.9, 66.8, 15.2.



(i) Zn, NaOH, H₂O, reflux for 1h; then 1-(2-ethoxyethoxy)-2-bromoethane, TBAB, reflux for 6h. (ii) *n*-butyllithium, THF, −78 °C, 1h, argon; then CBr₄, ambient temperature, 2h, argon. (iii-iv) Pd₂(dba)₃, P(*o*-Tol)₂, Toluene and DMF, 100 °C, 12h.

Scheme 1 Synthetic routes of P1 and P2

Synthesis of polymers (P1, P2)

The two polymers (P1 and P2 in Scheme 1) were prepared with the same procedure of coupling dibromide compounds with bis-(trimethylstannyl)-substituted compounds.

0.5 mmol of dibromide compound, 0.5 mmol of bis(trimethylstannyl)-substituted compound, 8 mL of toluene, and 2 mL of DMF were put into a two-necked flask. The mixture was purged with argon for 30 min, then Pd₂(dba)₃ (10 mg), and P(*o*-Tol)₃ (20 mg) were added, then the reaction was heated to 100 °C and stirred for 12 h under argon atmosphere. The mixture was cooled down to ambient temperature and the polymer was precipitated by addition of 150 mL methanol and filtered through a Soxhlet thimble, which was then subjected to Soxhlet extraction with methanol, hexane, and chloroform. The polymer was recovered as a solid sample from the chloroform fraction by rotary evaporation. The solid was dried under vacuum for 1 day to get the final product. The yields of the polymerization reactions were 79 % for P1 and 83 % for P2. P1: ¹H NMR (CDCl₃, 600 MHz), δ (ppm): 7.75–7.29 (br, 2H), 4.54–3.63 (br, 20H), 1.28 (br, 6H). P2: ¹H NMR (CDCl₃, 600 MHz), δ (ppm): 7.54–7.26 (br, 4H), 4.64–3.50 (br, 24H), 2.00 (br, 4H), 1.68–1.25 (br, 26H), 0.97 (br, 6H).

Results and discussion

Synthesis and characterization

The synthetic routes to the monomers and polymers are outlined in Scheme 1. Compound 1 was reduced by zinc dust in aqueous sodium hydroxide solution, when the reduction reaction was completed, 1-(2-ethoxyethoxy)-2-bromoethane was added with a catalytic amount of tetrabutylammonium bromide. After being refluxed for 12 h, compound 2 was obtained. Compound 3 was achieved by the bromination of compound 2 with *n*-butyl lithium and CBr₄. The polycondensation was carried out between organic tin compounds and bromides through the Stille coupling reaction. The monomers were characterized by ¹H NMR and ¹³C NMR. The polymers were dissolved only in chloroform, so the gel permeation chromatography data were not given.

Thermal stability

The thermal behavior of the polymers was evaluated by TGA and DSC in nitrogen with a heating rate of 10 °C/min. As depicted in Fig. 1, the two polymers showed good thermal stability. The 5 % weight loss of the polymers took place at 318 °C for P1 and 316 °C for P2. The good thermal stability of polymers prevents the deformation of

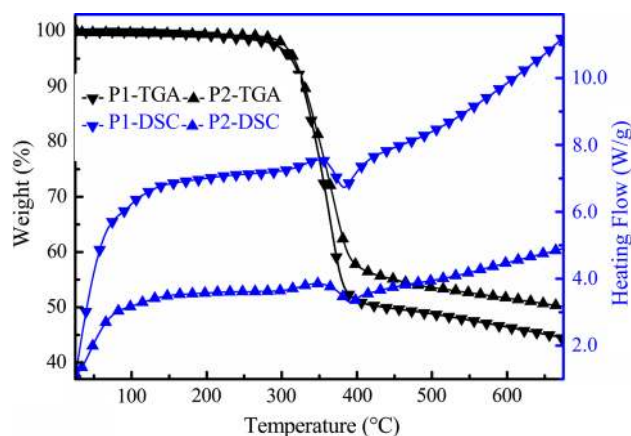


Fig. 1 TGA and DSC curves of P1 and P2

the polymer morphology and the degradation of the polymeric active layer under applied electric field in the solar cell devices. The polymers show no glass transition in DSC characterization during the scanning range from 30 to 350 °C at the rate of 10 °C/min under nitrogen flow. The thermal data are summarized in Table 1.

Optical properties

The optical absorption spectra of the polymers P1 and P2 in chloroform solution and in spin-coated thin films are shown in Fig. 2, and the corresponding absorption properties are summarized in Table 1. The polymers showed similar absorption profiles with two peaks from 400 to 600 nm, which should be ascribed to the π - π transitions in the polymer backbone. The absorption maxima of P1 and P2 in solution occurred at 520/486 and 524/485 nm respectively, whereas those in the thin films occurred at 536/497 and 536/494 nm. Obviously, the absorption spectra of the polymer films were red-shifted compared to those in solution, indicating the gain of planarity of the polymers and the strong interaction between polymer chains in the film states. The onsets of solid film absorption of P1 and P2 occurred at 566 and 560 nm. The onset absorption wavelength of P1 is higher than P2 which indicated that the efficient conjugation length of P1 was bigger than P2. This was consistent with the assumption that poly-ether side chains did not cause a detrimental steric twist of the polymer out of planarity which would be beneficial for the π - π stacking [38].

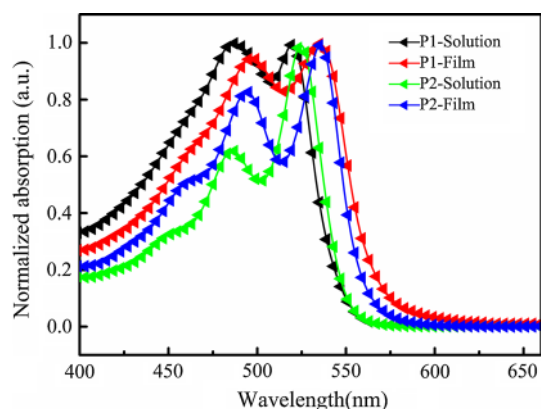
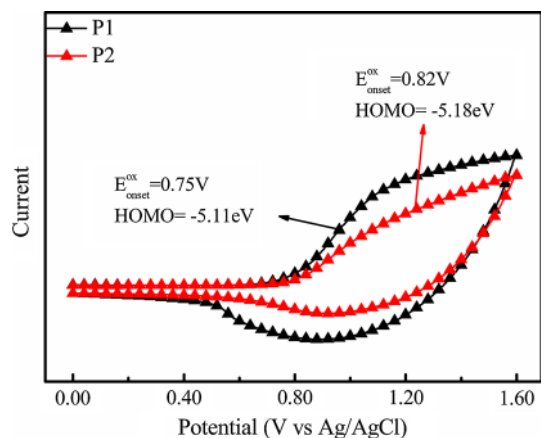
The optical band gaps (E_g^{opt}) deduced from the onset of absorption in the solid state are determined to be 2.19 eV for P1 and 2.21 eV for P2.

Electrochemical properties

To determine the highest occupied molecular orbital (HOMO) and the lowest unoccupied molecular orbital

Table 1 Optical, electrochemical, and thermal properties of P1 and P2

Polymer	λ_{\max} sol (nm)	λ_{\max} film (nm)	λ_{onset} film (nm)	$E_{\text{g}}^{\text{opt}}$ (eV)	$E_{\text{onset}}^{\text{ox}}$ (V)	HOMO (eV)	T_{d} (°C)
P1	520; 486	536; 497	566	2.19	0.75	-5.11	318
P2	524; 485	536; 494	560	2.21	0.82	-5.18	316

**Fig. 2** Normalized UV-Vis absorption spectra of P1 and P2 in solution and thin film**Fig. 3** Cyclic voltammograms of P1 and P2

(LUMO) energy levels, we investigated the electrochemical properties of the polymers by CV. A glassy carbon, modified with a polymer film by means of dip-coating, was used as the working electrode, whereas a platinum wire was used as the counter electrode and Ag/AgCl served as the reference electrode. CV were carried out in Bu₄NPF₆ (0.1 M)/acetonitrile electrolyte at room temperature under a nitrogen atmosphere at a scan rate of 50 mV/s. The CV plots of P1 and P2 are shown in Fig. 3, and the electrochemical properties are summarized in Table 1. The HOMO energy level of the polymers can be deduced from the oxidation onsets, assuming that the energy level of

ferrocene (Fc) is 4.8 eV below the vacuum level [39]. The redox potential of Fc/Fc⁺ internal reference vs. Ag/AgCl is 0.44 V, and the onset of oxidation for P1 and P2 occurred at 0.75 and 0.82 V in the same conditions, which corresponds to HOMO values of -5.11 and -5.18 eV, respectively. The LUMO levels of P1 and P2 were calculated from the optical band gaps and HOMO energy levels to be -2.92 and -2.97 eV.

Polymer solar cell performance

To elucidate the relationship between the conjugated polymers molecular structure and the solar cell devices performance, BHJ-type PSCs (ITO/PEDOT:PSS/active layer/Ca/Al) were fabricated based on the blends of P1 and P2 with PCBM. Figure 4a, b show the current density vs. voltage (*J*-*V*) curves under AM 1.5 illumination at 100 mW/cm². The representative characteristics of the PSCs devices are summarized in Table 2. In order to obtain optimized device performance, different weight ratios (2:1, 1:1, 1:2) of P1 or P2: PCBM were used. As shown in Fig. 4 and Table 2, the best device performance was obtained in a 1:1 polymer: PCBM weight ratio spin-cast from chloroform with $V_{\text{oc}} = 0.68$ V, $J_{\text{sc}} = 2.06$ mA/cm², FF = 50.55 %, PCE = 0.71 % for P1 and $V_{\text{oc}} = 0.68$ V, $J_{\text{sc}} = 4.86$ mA/cm², FF = 60.46 %, PCE = 2.00 % for P2. For comparison, a published homopolymer containing alkoxy side chain only was founded [37], and the photovoltaic parameters are $V_{\text{oc}} = 0.83$ V, $J_{\text{sc}} = 4.18$ mA/cm², FF = 45 %, and PCE = 1.56 %. From the characterized data, it is almost certain that the oxygen atom plays a crucial role to the photovoltaic properties and an optimal ratio of poly-ether side chain existed.

The external quantum efficiency (EQE) curves of the devices based on P1/PCBM and P2/PCBM (1:1, w/w) prepared under optimized conditions are shown in Fig. 4c. Both the devices exhibited photoresponse range from 300 to 600 nm, with the maximum EQE of 21.4 % for P1 and 61.5 % for P2. To confirm the accuracy of the photovoltaic measurements, the J_{sc} (2.03 mA/cm² for P1 and 4.81 mA/cm² for P2) were calculated from integration of the EQE curves, which agree well with the J_{sc} (2.06 mA/cm² for P1 and 4.86 mA/cm² for P2) obtained from the *J*-*V* measurements.

Fig. 4 **a, b** J - V curves of P1 and P2/PCBM-based solar cells with different ratios. **c** EQE curves of P1 and P2/PCBM (1:1, w/w)-based solar cells. **d** J - V characteristics of P1 and P2/PCBM (1:1, w/w) hole-only devices measured at ambient temperature

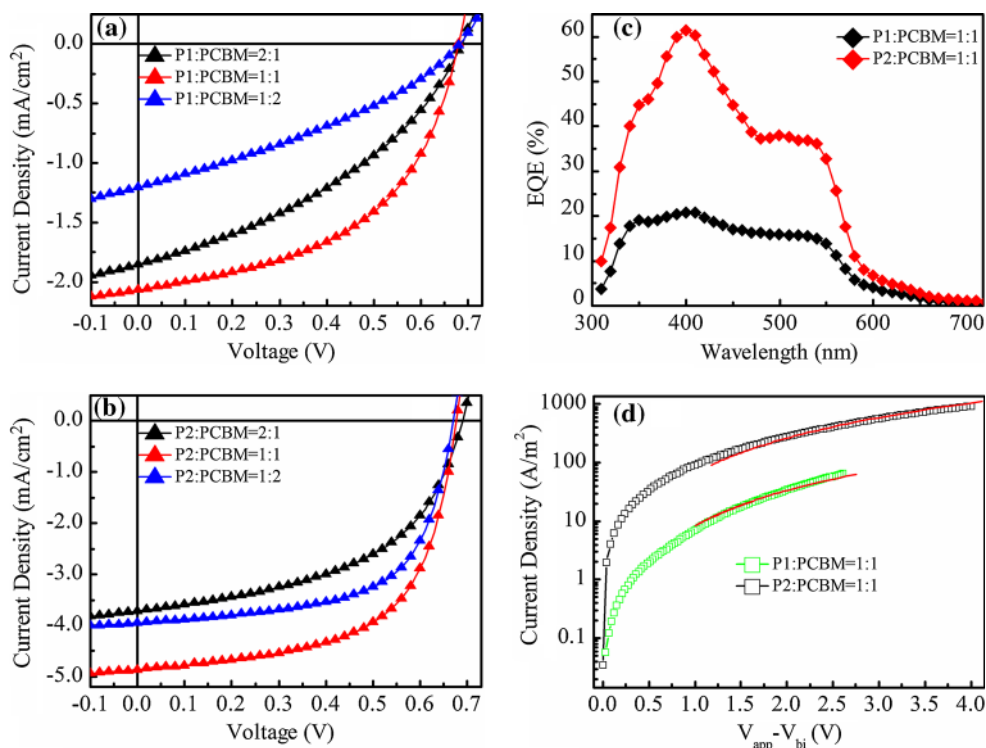


Table 2 Photovoltaic characteristics of P1, P2, and PCBM with different ratios

Polymers	Ratios (D:A)	V_{oc} (V)	J_{sc} (mA/cm ²)	FF (%)	PCE (%)
P1	2:1	0.68	1.85	38.58	0.49
	1:1	0.68	2.06	50.55	0.71
	1:2	0.68	1.20	33.98	0.28
P2	2:1	0.69	3.71	50.95	1.30
	1:1	0.68	4.86	60.46	2.00
	1:2	0.67	3.78	57.39	1.46

To further study the performance of the PSCs devices, the hole mobilities in the photosensitive layers were measured by the space-charge limited current (SCLC) method and the plots are shown in Fig. 4d. Hole-only devices were constructed with the structure of ITO/PEDOT:PSS/polymer:PCBM/MoO₃/Ag, and hole mobilities were calculated using the Mott–Gurney equation. For films of P1/PCBM and P2/PCBM, the SCLC mobilities were 3.69×10^{-6} and 2.92×10^{-5} cm²/Vs, respectively. The higher hole mobility of P2 guaranteed the increased FF than P1.

X-ray diffraction and atomic force microscopy (AFM)

As the morphology of phase-separated blends are key issues to enhance the devices efficiency, XRD patterns and AFM images of P1/PCBM (1:1, w/w) and P2/PCBM (1:1, w/w) blend films on ITO glass were carried out. The XRD patterns are shown in Fig. 5. P1 exhibited better crystallization capability with two peaks ($2\theta = 5.43^\circ$ and

$2\theta = 21.20^\circ$) compared with P2, which is probably caused by the higher mole ratio of poly-ether of P1 [40]. Those peaks after 25° correspond to the ITO substrate. However,

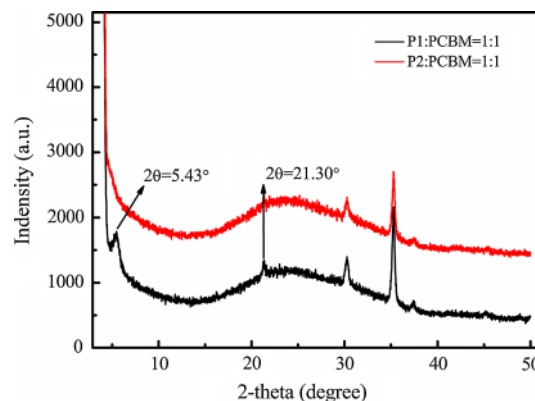


Fig. 5 X-ray diffraction patterns of P1:PCBM (1:1, w/w) and P2:PCBM (1:1, w/w)

better crystallization may lead to rather rough surface and fairly large domain size, which is unfavorable to charge separation and consequently limits device performance.

The surface morphologies of P1/PCBM and P2/PCBM blend films (1:1, w/w) are measured by AFM. As shown in Fig. 6, P1/PCBM blend film exhibits rather rough surface with a RMS value of 5.01 nm and fairly large domain size over 100 nm, which is unfavorable to charge separation and consequently limits device performance, so the best device based on P1 exhibited low J_{sc} of 2.06 mA/cm² and PCEs of 0.71 %. Nevertheless, for P2 with combining alkoxy and poly-ether chains, relatively smooth blend film surface along with appropriate domain size (20–40 nm) are realized with RMS value of 2.54 nm, indicating better nanoscale separation between the polymer and PCBM and more efficient percolation pathways that can facilitate charge transport to the respective electrodes and thereby lead to better performance. The best device based on P2 showed a PCE of 2.00 %.

Thin film field-effect transistors

The transfer characteristics curves of FETs based on P1 and P2 are shown in Fig. 7. The field-effect mobility (μ)

was obtained by plotting $I_{DS}^{1/2}$ vs. V_{GS} in the saturation regime (–40 V), using the equation

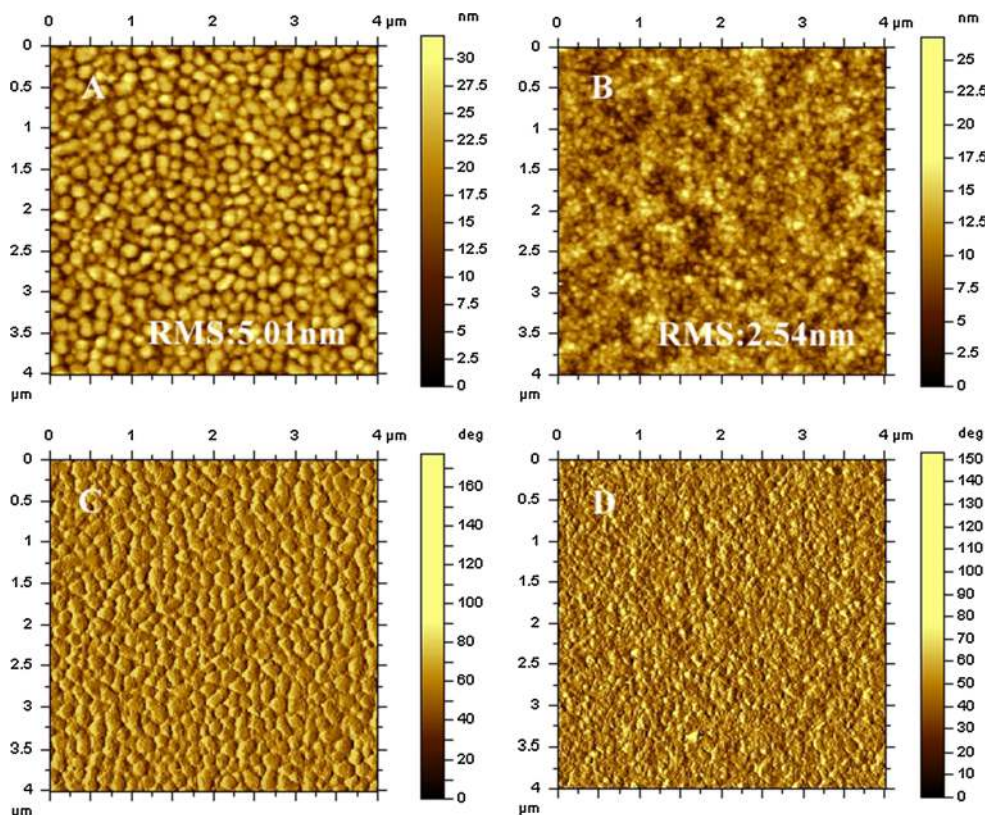
$$\mu = \frac{2L}{WC_i} \left[\frac{I_{DS}}{(V_{GS} - V_T)^2} \right],$$

where I_{DS} is the source-drain current, W is the channel width, L is the channel length, C_i is the capacitance of the dielectric, V_{GS} is the gate voltage, and V_T is the threshold voltage. The polymer P1 had mobility of 3.95×10^{-4} cm²/Vs, and the polymer P2 had a mobility of 6.18×10^{-4} cm²/Vs. P2 based FET devices show higher hole mobility than P1 device which agree with the SCLC results.

Solar cells stability

The stability of the best device based on P2 and PCBM blend was investigated. To simulate the encapsulated additions, the unencapsulated device was stored 16 days in nitrogen atmosphere under ambient temperature, and the changes of the photovoltaic parameters are shown in Fig. 8. As seen from Fig. 8, the V_{oc} drops about 1 %, J_{sc} drops 2.6 %, FF drops 3.0 %, and PCE drops 5.5 % after 16 days. These results demonstrated that the devices based

Fig. 6 AFM topography (a, b) and phase images (c, d) of P1/PCBM (1:1, w/w) blend film (a, c) and P2/PCBM (1:1, w/w) blend film (b, d)



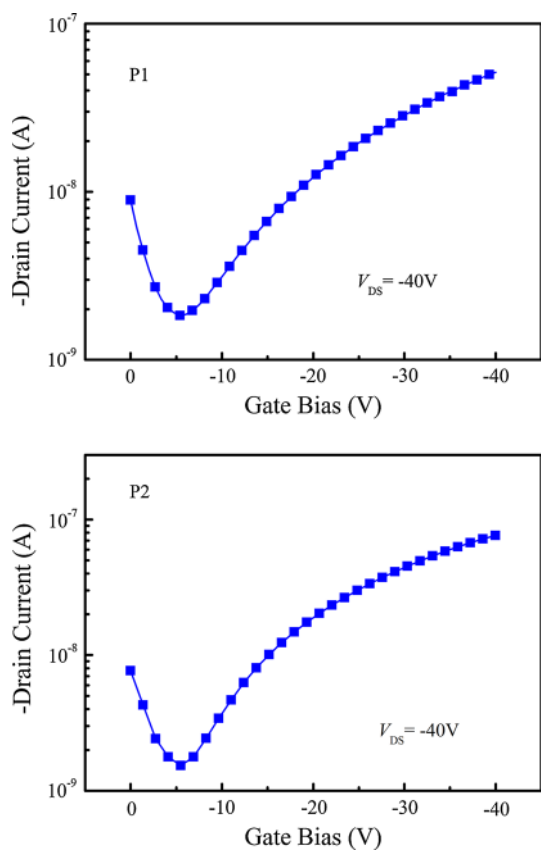


Fig. 7 I_D vs. V_G transfer characteristics of P1- and P2-based FET devices

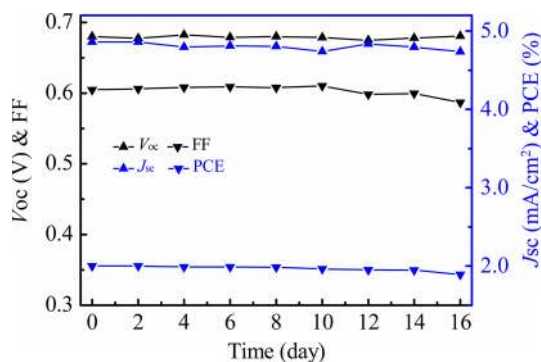


Fig. 8 Extract of the cell parameters up to 16 days aging for P2:PCBM (1:1, w/w) solar cell in nitrogen atmosphere

on P2 and PCBM would show good stability if they are well encapsulated.

Conclusions

In this paper, two BDT homopolymers with different mole ratios of poly-ether side chain were synthesized by Stille coupling reaction. Polymer with 100 % poly-ether side

chain (P1)-based solar cells show low PCEs of 0.71 % resulting from rough surface and fairly large domain size due to the high aggregation tendency of P1:PCBM thin film. Polymer with alternating poly-ether and alkoxy chained BDT (P2) and PCBM blend film shows smooth surface and appropriate domain size, which help to the hole transportation and photovoltaic performances. The PCEs of the devices based on P2 reached 2.00 % which is an acceptable result for a polymer donor with relatively high band gap (ca. 2.2 eV). Our preliminary results show that it is an effective way to modulate the morphology of donor and acceptor blend film by controlling the mole percentage of hydrophilic poly-ether side chain in polymer donor.

Acknowledgements The authors are deeply grateful to the National Natural Science Foundation of China (Project Nos. 21274134, 51173199, 61107090), New Century Excellent Talents in University (NCET-11-0473), Shandong Provincial Natural Science Foundation (ZR2011BZ007), Qingdao Municipal Science and Technology Program (11-2-4-22-hz, 13-1-4-200-jch) and Shenzhen Municipal Science and Technology Program (JCYJ20130401145617279) for financial support.

References

1. Yu G, Gao J, Hummelen JC, Wudl F, Heeger AJ (1995) Polymer photovoltaic cells: enhanced efficiencies via a network of internal donor–acceptor heterojunctions. *Science* 270:1789–1790
2. Brabec CJ (2004) Organic photovoltaics: technology and market. *Sol Energy Mater Sol Cells* 83:273–292
3. Günes S, Neugebauer H, Sariciftci NS (2007) Conjugated polymer-based organic solar cells. *Chem Rev* 107:1324–1338
4. Thompson BC, Fréchet JM (2008) Polymer-fullerene composite solar cells. *Angew Chem Int Ed* 47:58–77
5. Cheng YJ, Yang SH, Hsu CS (2009) Synthesis of conjugated polymers for organic solar cell applications. *Chem Rev* 109:5868–5923
6. Dennler G, Scharber MC, Brabec CJ (2009) Polymer-fullerene bulk-heterojunction solar cells. *Adv Mater* 21:1323–1338
7. Wen SG, Bao XC, Shen WF, Gu CT, Du ZK, Han LL, Zhu DQ, Yang RQ (2014) Benzodithiophene-based poly(aryleneethynylene)s: synthesis, optical properties, and applications in organic solar cell. *J Polym Sci, Part A: Polym Chem* 52:208–215
8. Liu Q, Bao XC, Wen SG, Du ZK, Han LL, Zhu DQ, Chen YH, Sun ML, Yang RQ (2014) Hyperconjugated side chained benzodithiophene and 4,7-di-2-thienyl-2,1,3-benzothiadiazole based polymer for solar cells. *Polym Chem* 5:2076–2082
9. Sista P, Kularatne RS, Mulholland ME, Wilson M, Holmes N, Zhou XJ, Dastoor PC, Belcher W, Rasmussen SC, Biewer MC, Stefan MC (2013) Synthesis and photovoltaic performance of donor–acceptor polymers containing benzo[1,2-b:4,5-b']dithiophene with thienyl substituents. *J Polym Sci, Part A: Polym Chem* 51:2622–2630
10. Zhang B, Yu L, Fan L, Wang N, Hu LW, Yang W (2014) Indolo[3,2-b]carbazole and benzofurazan based narrow band-gap polymers for photovoltaic cells. *New J Chem* 38:4587–4593
11. Tang WH, Hai JF, Shi GZ, Ma WL, Yu JS, Zhu EW, Bian LY (2014) Naphthodifuran alternating quinoxaline copolymers with a bandgap of 1.2 eV and their photovoltaic characterization. *New J Chem* 38:4816–4822

12. He ZC, Zhong CM, Su SJ, Xu M, Wu HB, Cao Y (2012) Enhanced power-conversion efficiency in polymer solar cells using an inverted device structure. *Nat Photon* 6:593–597
13. Szarko JM, Guo JC, Liang YY, Lee B, Rolczynski BS, Strzalka J, Xu T, Loser S, Marks TJ, Yu LP (2010) When function follows form: effects of donor copolymer side chains on film morphology and BHJ solar cell performance. *Adv Mater* 22:5468–5472
14. Piliago C, Holcombe TW, Douglas JD, Woo CH, Beaujuge PM, Fréchet JM (2010) Synthetic control of structural order in N-alkylthieno [3,4-c] pyrrole-4,6-dione-based polymers for efficient solar cells. *J Am Chem Soc* 132:7595–7597
15. Yang LY, Zhou HX, You W (2010) Quantitatively analyzing the influence of side chains on photovoltaic properties of polymer-fullerene solar cells. *J Phys Chem C* 114:16793–16800
16. Zhou HX, Yang LY, Xiao SQ, Liu SB, You W (2009) Donor-acceptor polymers incorporating alkylated dithienylbenzothiadiazole for bulk heterojunction solar cells: pronounced effect of positioning alkyl chains. *Macromolecules* 43:811–820
17. Svensson M, Zhang FL, Veenstra SC, Verhees WJ, Hummelen JC, Kroon JM, Inganäs O, Andersson MR (2003) High-performance polymer solar cells of an alternating polyfluorene copolymer and a fullerene derivative. *Adv Mater* 15:988–991
18. Chen MH, Hou JH, Hong ZR, Yang GW, Sista S, Chen LM, Yang Y (2009) Efficient polymer solar cells with thin active layers based on alternating polyfluorene copolymer/fullerene bulk heterojunctions. *Adv Mater* 21:4238–4242
19. Nguyen LH, Hoppe H, Erb T, Guenes S, Sariciftci NS (2007) Effects of annealing on the nanomorphology and performance of poly (alkylthiophene): fullerene bulk-heterojunction solar cells. *Adv Funct Mater* 17:1071–1078
20. Gadisa A, Oosterbaan WD, Vandewal K, Bolsée JC, Bertho S, D’Haen J, Lutsen L, Vanderzande D, Manca JV (2009) Effect of alkyl side-chain length on photovoltaic properties of poly (3-alkylthiophene)/PCBM bulk heterojunctions. *Adv Funct Mater* 19:3300–3306
21. Ko S, Verploegen E, Hong S, Mondal R, Hoke ET, Toney MF, McGehee MD, Bao ZN (2011) 3,4-Disubstituted polyalkylthiophenes for high-performance thin-film transistors and photovoltaics. *J Am Chem Soc* 133:16722–16725
22. Xin H, Kim FS, Jenekhe SA (2008) Highly efficient solar cells based on poly (3-butylthiophene) nanowires. *J Am Chem Soc* 130:5424–5425
23. Hou JH, Park MH, Zhang SQ, Yao Y, Chen LM, Li JH, Yang Y (2008) Bandgap and molecular energy level control of conjugated polymer photovoltaic materials based on benzo [1,2-b:4,5-b'] dithiophene. *Macromolecules* 41:6012–6018
24. Dou LT, Chang WH, Gao J, Chen CC, You JB, Yang Y (2012) A selenium-substituted low-bandgap polymer with versatile photovoltaic applications. *Adv Mater* 25:825–831
25. Li XH, Choy WC, Huo LJ, Xie FX, Sha WE, Ding BF, Guo X, Li YF, Hou JH, You JB (2012) Dual plasmonic nanostructures for high performance inverted organic solar cells. *Adv Mater* 24:3046–3052
26. Zhou HX, Yang LQ, Stuart AC, Price SC, Liu SB, You W (2011) Development of fluorinated benzothiadiazole as a structural unit for a polymer solar cell of 7% efficiency. *Angew Chem Int Ed* 123:3051–3054
27. Zhang MJ, Gu Y, Guo X, Liu F, Zhang SQ, Huo LJ, Russell TP, Hou JH (2013) Efficient polymer solar cells based on benzo-thiadiazole and alkylphenyl substituted benzodithiophene with a power conversion efficiency over 8%. *Adv Mater* 25:4944–4949
28. Chen HC, Chen YH, Liu CC, Chien YC, Chou SW, Chou PT (2012) Prominent short-circuit currents of fluorinated quinoxaline-based copolymer solar cells with a power conversion efficiency of 8.0%. *Chem Mater* 24:4766–4772
29. Liang YY, Xu Z, Xia JB, Tsai ST, Wu Y, Li G, Ray C, Yu LP (2010) For the bright future-bulk heterojunction polymer solar cells with power conversion efficiency of 7.4%. *Adv Mater* 22:E135–E138
30. Wang XC, Jiang P, Chen Y, Luo H, Zhang ZG, Wang HQ, Li XY, Yu G, Li YF (2013) Thieno [3,2-b] thiophene-bridged D- π -A polymer semiconductor based on benzo [1,2-b:4,5-b'] dithiophene and benzoxadiazole. *Macromolecules* 46:4805–4812
31. Huo LJ, Zhang SQ, Guo X, Xu F, Li YF, Hou JH (2011) Replacing alkoxy groups with alkylthienyl groups: a feasible approach to improve the properties of photovoltaic polymers. *Angew Chem Int Ed* 123:9871–9876
32. Dong Y, Hu XW, Duan CH, Liu P, Liu SJ, Lan LY, Chen DC, Ying L, Su SJ, Gong X, Huang F, Cao Y (2013) A series of new medium-bandgap conjugated polymers based on naphtho [1,2-c:5,6-c] bis (2-octyl-[1,2,3] triazole) for high-performance polymer solar cells. *Adv Mater* 25:3683–3688
33. Chang WH, Gao J, Dou LT, Chen CC, Liu YS, Yang Y (2013) Side-chain tunability via triple component random copolymerization for better photovoltaic polymers. *Adv Energy Mater* 4: DOI:10.1002/aenm.201300864
34. Yang YC, Wu RM, Wang X, Xu XP, Li ZJ, Li K, Peng Q (2014) Isoindigo fluorination to enhance photovoltaic performance of donor-acceptor conjugated copolymers. *Chem Commun* 50:439–441
35. Li WW, Furlan A, Roelofs WC, Hendriks KH, van Puijssse GW, Wienk MM, Janssen RA (2014) Wide band gap diketopyrrolopyrrole-based conjugated polymers incorporating biphenyl units applied in polymer solar cells. *Chem Commun* 50:679–681
36. Cabanetos C, El Labban A, Bartelt JA, Douglas JD, Mateker WR, Fréchet JM, McGehee MD, Beaujuge PM (2013) Linear side chains in benzo [1,2-b:4,5-b'] dithiophene-thieno [3,4-c] pyrrole-4,6-dione polymers direct self-assembly and solar cell performance. *J Am Chem Soc* 135:4656–4659
37. Lee D, Hubijar E, Kalaw GJD, Ferraris JP (2012) Enhanced and tunable open-circuit voltage using dialkylthio benzo [1,2-b:4,5-b'] dithiophene in polymer solar cells. *Chem Mater* 24:2534–2540
38. Lee JK, Ma WL, Brabec CJ, Yuen J, Moon JS, Kim JY, Lee K, Bazan GC, Heeger AJ (2008) Processing additives for improved efficiency from bulk heterojunction solar cells. *J Am Chem Soc* 130:3619–3623
39. Peet J, Kim J, Coates NE, Ma WL, Moses D, Heeger AJ, Bazan GC (2007) Efficiency enhancement in low-bandgap polymer solar cells by processing with alkane dithiols. *Nat Mater* 6:497–500
40. Lu K, Fang J, Zhu XW, Yan H, Li DH, Yang YL, Wei ZX (2013) A facile strategy to enhance the fill factor of ternary blend solar cells by increasing charge carrier mobility. *New J Chem* 37:1728–1735